INTERNATIONAL JOURNAL FOR NUMERICAL METHODS IN FLUIDS
Int. J. Numer. Meth. Fluids 2001; **35**: 299–317

A numerical method for the determination of weakly non-hydrostatic non-linear free surface wave propagation

Z. Li[a,*] and B. Johns[b]

[a] *Ocean Applications, The Meteorological Office, London Road, Bracknell, U.K.*
[b] *Department of Computing Information Systems and Mathematics, London Guildhall University, 100 Minories, London, U.K.*

SUMMARY

A numerical method is described that may be used to determine the propagation characteristics of weakly non-hydrostatic non-linear free surface waves over a general, bottom topography. In shallow water of constant undisturbed depth, such waves are equivalent to the familiar cnoidal waves characterized by sharp crests and relatively flat troughs. For a certain range of parameters, these propagate without change of form by virtue of the weakly non-hydrostatic balance in the vertical momentum equation. Effectively, this counters the tendency for the non-linearity in a purely hydrostatic theory to lead to a continuously deforming surface wave profile. The realistic representation furnished by cnoidal wave theory of free surface waves in the shallow near-shore zone has led to its utilization in evaluating their propagation characteristics. Nonetheless, the classic analytical theory is inapplicable to the case of wave propagation over a sloping beach or off-shore sand bar topography. Under these conditions, a local change in form of the surface wave profile is anticipated before the waves break and knowing this is required in order to evaluate fully the propagation process. The efficacy of the numerical method is first demonstrated by comparing the solution for water of constant depth with the evaluation of the analytical solution expressed in terms of the Jacobian elliptic function *cn*. The general method described in the paper is then illustrated by experiments to determine the change in profile of weakly non-hydrostatic non-linear surface waves propagating over bed forms representative of those found in shallow coastal seas. Copyright © 2001 John Wiley & Sons, Ltd.

KEY WORDS: cnoidal waves; free surface; non-hydrostatic; irregular bottom topography

1. INTRODUCTION

The reflection of surface wave energy by undulations on the sea floor is an important problem in near-shore ocean dynamics. An extensive literature exists and one method of treatment applied obtains a solution of the governing equations for the motion of a free surface fluid by

* Correspondence to: Room 242, Ocean Applications, The Meteorological Office, London Road, Bracknell, Berks., U.K.

Received July 1999
Revised January 2000

an expansion in powers of the amplitude of the bottom undulations. This approach, which also involves a prescription of surface waves of small amplitude, has been pursued by Davies [1,2] in connection with sinusoidal bottom undulations. Other analytical treatments of the problem by Newman [3] and Miles [4] have been restricted to wave propagation over simple topographic variations, such as a step change in the depth. Again, the solution is obtained from a consideration of linearized equations.

However, in a shallow near-shore sea, the classic Stokes wave solution ultimately fails to yield a valid approximation to the free surface profile. In such a region, the wave propagation process becomes inherently non-linear and, in general, recourse must be made to a numerical treatment. For waves with an amplitude a and a wavelength ℓ in water of equilibrium depth h, a relevant parameter is $U = a\ell^2/h^3$. As documented by Lighthill [5], the waves are unable to propagate without change of form for $U > 16$, but for $U < 16$, non-deforming periodic waves are possible. In the limit as $U \to 0$, the Stokes wave theory becomes applicable. Clearly, for fixed values of ℓ and h, an increase in the value of U is equivalent to an increase in the non-linearity.

When $U \gg 16$, a numerical treatment of the non-linear shallow water equations may be expected to yield the propagation characteristics up until the formation of a discontinuity in the wave profile. This is relatively easy to implement even in the case of a non-uniform equilibrium depth of water. However, when $U < 16$, but with $U = O(1)$, non-linear propagation with an unchanging form involves a treatment of a weakly non-hydrostatic system. When the water is of constant equilibrium depth, analytical theories are available, such as that originally developed by Korteweg and de Vries (KdV) [6], and this leads to the classic cnoidal waves described by Lamb [7]. When the equilibrium depth is variable, such as in the near-shore zone, an analytical approach is no longer available and any assessment of wave energy reflection must be made by a numerical treatment.

In the present paper, the numerical method described by Johns [8] for the determination of the steady non-hydrostatic free surface flow over topography has been generalized to the case of an unsteady frictionless flow. The intention here is principally to demonstrate the validity of the method by comparing the results of a prototype integration with the analytical solution obtained by the use of the KdV equation. The method, which has widespread applicability to the evaluation of non-linear wave reflection by bottom topographical features, is first tested against the classic analytical solution for a constant depth. Numerical experiments are then described to determine the deforming effect of an irregular bottom topography on cnoidal wave propagation.

Unlike procedures based on the use of approximate equations for weakly non-hydrostatic systems by Nadiga *et al*. [9], which relate only to the propagation of a topographically forced solitary wave and are not immediately applicable to the case of an input of a periodic wave train of cnoidal waves, the method to be described utilizes exact equations. Moreover, it is readily applied to the propagation of a spectrum of incoming wave components and also to the determination of the interaction between waves and an incoming steady current. At the expense of a greater computational effort, the model may readily be extended to the case of two horizontal space dimensions. Equally importantly, unlike an application of the approximate dimension-reduced equation in Reference [9], the present method leads to the determination of the vertical current structure beneath waves—an aspect of paramount importance in

future applications of the model to the suspended sediment transport. Indeed, the method is currently in an advanced stage of development by the authors to the case of wave propagation over variable bottom topography when the flow conditions are turbulent and can be simulated by the type of closure scheme used in Reference [8]. Such an application leads to being able to model intermittent flow separation from the bottom topography and vortex shedding during a wave cycle. In this form, following Li and Johns [10], the method is also potentially applicable to the calculation of surf zone dynamics.

Reference is made to recent work by Stansby and Zhou [11], relating to the modelling of non-hydrostatic flow over topography. Specifically, this applies to steady flow, although the authors are extending it to wave-induced flows. Compared with the work reported in Reference [8], their approach utilizes a numerical procedure based on the determination of the non-hydrostatic pressure by solving a Poisson equation; this being the most computational expensive part of the calculation. In contrast, the method in the present paper dispenses with such a technique and instead invokes a doubly iterative method to complete each time step. It seems to the present authors that both procedures are likely to lead to an equivalent computational effort.

2. FORMULATION

A two-dimensional analysis domain is chosen in which the origin, O, is situated in the equilibrium level of the free surface of the water. All conditions are referred to rectangular Cartesian co-ordinates. In these, the axis Ox points downstream in the direction of wave propagation and Oz is measured vertically upwards. At time t, the disturbed position of the free surface of the water is at $z=\zeta(x, t)$ and a general immobile bottom topography corresponds to $z=-h(x)$. The equations of motion of a frictionless incompressible fluid, in which velocity is denoted by (u, w), density by ρ and pressure by p, then have the flux form

$$\frac{\partial u}{\partial t}+\frac{\partial(uu)}{\partial x}+\frac{\partial(uw)}{\partial z}=-\frac{1}{\rho}\frac{\partial p}{\partial x} \tag{2.1}$$

and

$$\frac{\partial w}{\partial t}+\frac{\partial(uw)}{\partial x}+\frac{\partial(ww)}{\partial z}=-g-\frac{1}{\rho}\frac{\partial p}{\partial z} \tag{2.2}$$

The equation of continuity has either of the equivalent forms

$$\frac{\partial u}{\partial x}+\frac{\partial w}{\partial z}=0 \tag{2.3}$$

or

$$\frac{\partial \zeta}{\partial t}+\frac{\partial}{\partial x}\left(\int_{-h}^{\zeta} u \, \mathrm{d}z\right)=0 \tag{2.4}$$

Integrating Equation (2.2) from a general depth, z, to the free surface, where the pressure is atmospheric and is equal to p_{a}, we obtain

$$\frac{p}{\rho}=\frac{p_{\mathrm{a}}}{\rho}+g(\zeta-z)+\frac{\partial}{\partial t}\int_{z}^{\zeta} w \, \mathrm{d}z+\frac{\partial}{\partial x}\int_{z}^{\zeta} uw \, \mathrm{d}z-w^2 \tag{2.5}$$

The partial hydrodynamic kinematic pressure, P, is then defined by

$$P=\frac{\partial}{\partial x}\int_{z}^{\zeta} uw \, \mathrm{d}z-w^2 \tag{2.6}$$

in which case, Equation (2.1) may be written in the form

$$\frac{\partial}{\partial t}\left(u+\frac{\partial}{\partial x}\int_{z}^{\zeta} w \, \mathrm{d}z\right)+\frac{\partial(uu)}{\partial x}+\frac{\partial(uw)}{\partial z}=-\frac{\partial P}{\partial x}-g\frac{\partial \zeta}{\partial x} \tag{2.7}$$

where the atmospheric pressure has been taken as constant. Thus, a new prognostic variable, χ, may be defined by

$$\chi=u+\frac{\partial}{\partial x}\int_{z}^{\zeta} w \, \mathrm{d}z \tag{2.8}$$

A transformation is then made to the topography following σ co-ordinates defined in Reference [8]. The dangers of this procedure when applied in a numerical model are well known in the case of flow over steep topography and are documented by Stelling and van Kester [12]. However, our applications in this paper will never involve a bottom topography that is steeper than that of the free surface undulations and, when the undisturbed fluid depth is uniform, we show that the derived numerical solution compares excellently with the analytical solution available in this case. The transformation yields

$$\frac{\partial \tilde{\chi}}{\partial t}+\frac{\partial(u\tilde{u})}{\partial x}+\frac{\partial(\omega\tilde{u})}{\partial \sigma}+\frac{\partial}{\partial \sigma}[(\tilde{\chi}-\tilde{u})\sigma_t]=-H\frac{\partial P}{\partial x}-(h_x-\sigma H_x)\frac{\partial P}{\partial \sigma}-gH\frac{\partial \zeta}{\partial x} \tag{2.9}$$

In Equation (2.9) subscripts denote differentiations; H denotes the total depth, $\zeta+h$; $\tilde{\chi}$ and $\tilde{u}$ denote $H\chi$ and Hu respectively. The independent variables are x, σ and t, where $\sigma=(z+h)/H$. The 'vertical velocity' is $\omega=\sigma_t+u\sigma_x+w\sigma_z$, where the subscripts again denote differentiations, and the prognostic variable, $\tilde{\chi}$, in Equation (2.9) transforms to

$$\tilde{\chi}=\tilde{u}+H\frac{\partial}{\partial x}\int_{\sigma}^{1} Hw \, \mathrm{d}\sigma-H(h_x-\sigma H_x)w \tag{2.10}$$

The general bottom topography and the free surface of the water now correspond to $\sigma = 0$ and $\sigma = 1$ respectively. Accordingly, the kinematic boundary conditions at these levels yield $\omega = 0$ at $\sigma = 0$ and $\sigma = 1$.

Following Reference [8], transformation of Equation (2.4) yields

$$\frac{\partial \zeta}{\partial t} + \frac{\partial}{\partial x} \int_0^1 \tilde{u} \, \mathrm{d}\sigma = 0 \tag{2.11}$$

and by continuity, since $\omega = 0$ at $\sigma = 0$, a diagnostic determination of ω leads to

$$H\omega = -\frac{\partial}{\partial x} \int_0^\sigma H(u - \bar{u}) \, \mathrm{d}\sigma \tag{2.12}$$

where

$$\bar{u} = \int_0^1 u \, \mathrm{d}\sigma \tag{2.13}$$

The vertical velocity, w, may then be deduced from

$$w = H\omega - \sigma \frac{\partial}{\partial x} \int_0^1 \tilde{u} \, \mathrm{d}\sigma - \left(\frac{\partial h}{\partial x} - \sigma \frac{\partial H}{\partial x} \right) u \tag{2.14}$$

and the partial hydrodynamic pressure is determined from

$$P = \frac{\partial}{\partial x} \int_\sigma^1 \tilde{u} w \, \mathrm{d}\sigma - w^2 - \left(\frac{\partial h}{\partial x} - \sigma \frac{\partial H}{\partial x} \right) uw \tag{2.15}$$

Additionally, further conditions are required at each end of the analysis domain. At $x = 0$, an appropriate input condition must be applied that supports an inwardly propagating train of surface waves. At $x = L$, a condition must be applied that allows for the untrammelled outward radiation of the wave train after modification by propagation over the prescribed bed form. The form of these is determined by prescribing segments of the flat-bed analysis domain adjacent to both $x = 0$ and $x = L$ in which the pressure is strictly hydrostatic. This then allows for the specification of radiation conditions based upon those used in Reference [8]. Specifically, if ΔL is the length of each segment, the pressure is taken to be strictly hydrostatic for $0 \le x \le \Delta L$ and $L - \Delta L \le x \le L$. Then, a radiation condition is prescribed at $x = 0$ in which

$$\bar{u} + \left(\frac{g}{h} \right)^{1/2} \zeta = 2u_0 \sin(ft) \tag{2.16}$$

where u_0 and f denote a velocity amplitude and the radian frequency of the incoming waves, respectively. As well as supporting the input of the wave train into the analysis domain, Equation (2.16) is also consistent (subject to the implied approximations) with the possible

outward transmission across $x = 0$ of a part of the wave response reflected from an irregular bed form. In a similar manner, a further radiation condition is applied at $x = L$ in which

$$\bar{u} - \left(\frac{g}{h}\right)^{1/2} \zeta = 0 \tag{2.17}$$

Clearly, Equations (2.16) and (2.17) are unaltered in form by the transformation to the σ co-ordinates.

3. NON-DIMENSIONALIZATION

Before proceeding to the numerical solution of the non-hydrostatic equations, it is expedient to identify the relevant dimensionless parameters determining the form of the solution. To accomplish this, it is necessary to specify a horizontal length scale associated with the waves. This is denoted by b, and is related to the wave period $t_p = 2\pi/f$ and the equilibrium depth, h_0, at $x = 0$ by

$$b = t_p(gh_0)^{1/2} \tag{3.1}$$

Therefore, b is the wavelength of small amplitude shallow water waves, with period t_p in water of uniform depth h_0.

The replacement of the dimensional variables χ, $\tilde{\chi}$, u, w, ω, $\tilde{u}$, x, L, t, (H, h, ζ) and P by their scaled counterparts $u_0\chi$, $h_0u_0\tilde{\chi}$, u_0u, $(h_0/b)u_0w$, $(u_0/b)\omega$, $h_0u_0\tilde{u}$, bx, bL, $(b/u_0)t$, $h_0(H, h, \zeta)$ and $(h_0u_0/b)^2P$ then allows a reduction of the problem to a dimensionless form in which Equations (2.11) and (2.9) become

$$\frac{\partial H}{\partial t} + \frac{\partial}{\partial x}\int_0^1 \tilde{u}\, \mathrm{d}\sigma = 0 \tag{3.2}$$

and

$$\begin{aligned} &\frac{\partial \tilde{\chi}}{\partial t} + \frac{\partial(u\tilde{u})}{\partial x} + \frac{\partial(\omega\tilde{u})}{\partial \sigma} + \frac{\partial}{\partial \sigma}\left[(\tilde{\chi} - \tilde{u})\left(-\frac{\sigma H_t}{H}\right)\right] \\ &= -\lambda\left[H\frac{\partial P}{\partial x} + \left(\frac{\partial h}{\partial x} - \sigma\frac{\partial H}{\partial x}\right)\frac{\partial P}{\partial \sigma}\right] - H\mu\left[\frac{\partial H}{\partial x} - \frac{\partial h}{\partial x}\right] \end{aligned} \tag{3.3}$$

where

$$\lambda = (h_0/b)^2, \qquad \mu = gh_0/u_0^2 \tag{3.4}$$

The non-dimensionalization of Equation (2.10) leads to

$$\tilde{\chi} = \tilde{u} + \lambda\left[H\frac{\partial}{\partial x}\int_{\sigma}^{1} Hw \, \mathrm{d}\sigma - H(h_x - \sigma H_x)w \right] \tag{3.5}$$

while Equations (2.12), (2.14) and (2.15) are unchanged in form. The dimensionless forms of Equations (2.16) and (2.17) are

$$\bar{u} + (\mu/h)^{1/2}\zeta = 2\sin(ft) \quad \text{at } x = 0 \tag{3.6}$$

and

$$\bar{u} - (\mu/h)^{1/2}\zeta = 0 \quad \text{at } x = L \tag{3.7}$$

respectively. In Equation (3.6), f (scaled by u_0/b) now refers to the dimensionless radian frequency of the incoming waves.

In terms of this formulation, a representative expression for U, as defined in Section 1, may be obtained in which $a = u_0(h_0/g)^{1/2}$, $\ell = b$, $h = h_0$ and is then given by

$$U = \lambda^{-1}\mu^{-1/2} \tag{3.8}$$

4. ANALYTICAL SOLUTION FOR A CONSTANT EQUILIBRIUM DEPTH

When the equilibrium depth is constant, an analytical solution of the weakly non-hydrostatic non-linear problem is available using the KdV theory [6]. The application of this to obtain the lowest-order approximation to periodic waves that may propagate without change of form is described by Lamb [7]. The relevant formulas for the solution of the dimensionless problem are summarized here with a view to comparing the evaluation of these with the numerical solution. If ζ_a and ζ_b are the maximum dimensionless vertical displacements of the wave crest and wave trough from the equilibrium level respectively, the dimensionless wave elevation is given by

$$\zeta = -\zeta_b + (\zeta_a + \zeta_b)cn^2[\beta(x - c\mu^{1/2}t),\ k] \tag{4.1}$$

In Equation (4.1), cn denotes a Jacobian elliptic function with modulus k and

$$\beta = \frac{\sqrt{3}(\zeta_a + \zeta_c)^{1/2}}{2\sqrt{\lambda}c} \tag{4.2}$$

where $\zeta_c = -\zeta_a + (\zeta_a + \zeta_b)/k^2$. The dimensionless phase speed, c (scaled by $(gh_0)^{1/2}$) is given by

$$c^2 = 1 + \zeta_a - \zeta_b - \zeta_c \tag{4.3}$$

Finally, the modulus k is determined from the condition that the waves form a periodic train, which leads to the non-algebraic equation

$$\xi[K(k) - E(k)] - k^2 K(k) = 0 \tag{4.4}$$

where $\xi = 1 + \zeta_b/\zeta_a$. K and E are the first and second complete elliptic integrals respectively, defined in Reference [13] by

$$K(k) = \int_0^{\pi/2} (1 - k^2 \sin^2 \theta)^{-1/2} \, \mathrm{d}\theta \tag{4.5}$$

and

$$E(k) = \int_0^{\pi/2} (1 - k^2 \sin^2 \theta)^{1/2} \, \mathrm{d}\theta \tag{4.6}$$

For cnoidal waves to exist, Equation (4.4) must have a root such that $0 < k < 1$ and this clearly imposes a restriction on the admissible values of ζ_a and ζ_b.

5. NUMERICAL METHOD

With given initial fields of values for u, $\tilde{u}$, $\tilde{\chi}$ and H (which are arbitrary and are efficiently, but not necessarily, derived from the strictly hydrostatic solution for shallow water surface waves), an initial update of H is obtained by application of Equation (3.2). A first approximation is determined for the partial hydrodynamic kinematic pressure P, by use of Equation (2.15) with the value of w being determined from the dimensionless form of Equation (2.14). The implied values of P are then substituted into Equation (3.3) and the advance of $\tilde{\chi}$ through an initial time step is computed. The next stage in the solution process is to determine the corresponding updated values of $\tilde{u}$ and w through the use of Equation (3.5) and the dimensionless forms of Equations (2.12) and (2.14). This is done by the invocation of an iterative procedure in which an initial estimate of w is made by using the value corresponding to the previous time step. Substituting for w in Equation (3.5), the implied value of $\tilde{u}$ (and therefore u) is then determined in terms of the update of $\tilde{\chi}$. An improvement for w is obtained by substituting this value of $\tilde{u}$ into Equation (2.12) and (2.14). The process is repeated by inserting the improvement for w in Equation (3.5) and deducing a correspondingly improved value of $\tilde{u}$. The iteration process, when convergent, is terminated when successive approximations to $\tilde{u}$ are within a specified tolerance (here, taken as a maximum relative difference of 0.01 per cent). In the present application, this is always achieved in fewer than ten iterations. The ensuing numerical values of the field variables are then used to re-estimate P from Equation (2.15). Subsequently, Equation (3.3) is applied to re-compute the updated value of $\tilde{\chi}$, and the entire doubly iterative procedure is repeated until two successive approximations to P are obtained that have a maximum difference within a specified tolerance (taken here to be equivalent to less than a 1 per cent relative difference between successive iterates). When this is achieved, the first time step has been completed. The second time step is initiated with an update of H by application of Equation (3.2). The doubly iterative process, involving the repeated use of Equation (3.3), is applied for this and all subsequent time steps, but with the first approximation to P being

taken as the final iterated field from the previous time step. Ultimately, an effectively oscillatory response is obtained in which the computed fields of u and P reproduce themselves from one complete cycle of the integration to the next.

The above solution procedure is implemented by forming a discretized finite difference version of the continuous equations. In this, we define discrete values of x and σ by writing

$$x = x_i = (i-1)\Delta x; \quad i = 1, 2, 3, \ldots, m, \quad \Delta x = L/(m-1)$$

$$\sigma = \sigma_j = (j-1)\Delta\sigma; \quad j = 1, 2, 3, \ldots, n, \quad \Delta\sigma = 1/(n-1) \tag{5.1}$$

Discrete values of t are defined by

$$t = t_k = k\Delta t, \quad k = 1, 2, \ldots \tag{5.2}$$

where the time step Δt has to be chosen so as to be consistent with computational stability.

For any variable X we write

$$X(x_i, \sigma_j, t_k) = X_{ij}^k \tag{5.3}$$

Hence, in Equation (3.2), we may evaluate the integral in discrete form and write

$$I_i^k = \left[\int_0^1 \tilde{u}\, \mathrm{d}\sigma\right]_i^k = \frac{1}{2}\Delta\sigma \sum_{j=1}^{n-1} (\tilde{u}_{ij}^k + \tilde{u}_{ij+1}^k) \tag{5.4}$$

In order to describe the finite difference equations, we define difference operators by

$$\Delta_t X = \frac{X_{ij}^{k+1} - X_{ij}^k}{\Delta t}$$

$$\delta_x X = \frac{X_{i+1j}^k - X_{i-1j}^k}{2\Delta x}$$

$$\Delta_\sigma X = \frac{X_{ij+1}^k - X_{ij}^k}{\Delta\sigma} \tag{5.5}$$

$$\nabla_\sigma X = \frac{X_{ij}^k - X_{ij-1}^k}{\Delta\sigma}$$

$$\delta_\sigma X = \frac{X_{ij+1}^k - X_{ij-1}^k}{2\Delta\sigma}$$

A further operator E_σ is defined by

$$E_\sigma = \Delta_\sigma \quad \text{for } j = 1$$

$$E_\sigma = \delta_\sigma \quad \text{for } 1 < j < n \tag{5.6}$$

$$E_\sigma = \nabla_\sigma \quad \text{for } j = n$$

Finally, averaging and shift operations are defined by

$$\bar{X}^x = \frac{1}{2}(X^k_{i+1j} + X^k_{i-1j})$$

$$S_t X = X^{k+1}_{ij} \tag{5.7}$$

Equation (3.2) then leads to

$$\Delta_t H + \delta_x I = 0 \tag{5.8}$$

which is applied for $i = 3, 5, 7, \ldots, m-2$, and this provides a means of advancing the value of H through the time increment Δt. The index 'i' runs through odd values because of the staggered nature of the grid.

For $i = 1$ and $i = m$, H is not determined by Equation (5.8). For these values of i, H is obtained through the use of Equations (3.6) and (3.7) and these are discretized in a way that implies their application at $x = \Delta x$ and $x = L - \Delta x$. They are written in the form

$$H^{k+1}_1 = -H^{k+1}_3 + 2\left\{h_2 + \left(\frac{\mu}{h_2}\right)^{-1/2}[2\sin(ft_{k+1}) - \bar{u}^k_2]\right\} \tag{5.9}$$

and

$$H^{k+1}_m = -H^{k+1}_{m-2} + 2\left(h_{m-1} + \left(\frac{\mu}{h_{m-1}}\right)^{-1/2}\bar{u}^k_{m-1}\right) \tag{5.10}$$

Equation (3.3) is discretized according to

$$\begin{aligned}&\Delta_t\tilde{\chi} + \delta_x(\overline{u\tilde{u}}^x) + E_\sigma(\bar{\omega}^x\tilde{u}) + E_\sigma\left[(\tilde{\chi} - \tilde{u})\frac{\sigma}{H}\delta_x I\right]\\ &= -\lambda S_t[H\delta_x P + \delta_x\{h - \sigma H\}E_\sigma P] - \mu S_t[H\delta_x(H - h)]\end{aligned} \tag{5.11}$$

which is applied for $i = 2, 4, 6, \ldots, m-1$ and $j = 1, 2, 3, \ldots, n$, with a local linearization of the horizontal advective terms when $i = 2$ and $i = m-1$. It should be noted that this linearization is consistent with the use of the radiation boundary conditions (5.9) and (5.10), which are applied in the prescribed hydrostatic zones adjacent to $x = 0$ and $x = L$. Essentially, the scheme is derived from that described by Sielecki [14] and yields second-order accuracy in the time discretization.

In connection with the implementation of Equation (5.11) and the iterative determination of $\tilde{u}$ and w from the resulting update of $\tilde{\chi}$, the dimensionless forms of Equations (2.12) and (2.14) lead to

$$w = -\delta_x\left[\int_0^\sigma \{\tilde{u} - \bar{u}S_t(H)\}\,\mathrm{d}\sigma + \sigma\int_0^1 \tilde{u}\,\mathrm{d}\sigma\right] - u\delta_x\{h - \sigma S_t(H)\} \tag{5.12}$$

where u is determined from the value of $\tilde{u}/(\bar{\zeta}^x + h)$.

Equation (3.5) is discretized according to

$$\tilde{\chi} = \tilde{u} + \lambda\left[S_t(H)\delta_x\int_\sigma^1 S_t(H)w\,\mathrm{d}\sigma - wS_t\{H\delta_x(h - \sigma H)\}\right] \tag{5.13}$$

In Equations (5.12) and (5.13), the integrals are evaluated by replacing them with discrete sums. It is, therefore, clearly seen that the strictly hydrostatic case corresponds to $\lambda = 0$. Thus, it is anticipated that the iterative procedure to determine $\tilde{u}$ and w by simultaneous solutions of Equations (5.12) and (5.13) should be convergent for sufficiently small values of λ.

In connection with the iterative determination of P, the dimensionless form of Equation (2.15) is discretized according to

$$P = \delta_x\left(\int_\sigma^1 \tilde{u}w\,\mathrm{d}\sigma\right) - w^2 - uwS_t[\delta_x(h - \sigma H)] \tag{5.14}$$

with the integral again being replaced by a discrete sum. It is apparent, therefore, that an evaluation of P cannot be made when either $i = 2$ or $i = m - 1$. Such an evaluation, however, is never required, since these points lie within the prescribed hydrostatic zones, where $P \equiv 0$.

Finally, the practical numerical implementation of this method of solution has been found to lead to an aliasing phenomenon characteristic of non-linear problems. This is overcome and computational stability is achieved by the application of periodic selective smoothing of the evolving field variables. In addition to this, however, a problem related to the amplification of numerical noise has been encountered in the iterative solutions of Equations (5.12) and (5.13). This has also been overcome by the application of a selective smoothing operator to the vertical velocity, w, as it is determined after each iteration. This smoothing operation is unconnected with the attainment of computational stability in the integrations and is solely related to the attainment of convergence in the iteration procedure to determine w. These procedures are described further in Appendix A. The overall effect of the smoothing on the final fields is assessed when the solution for a constant equilibrium depth is compared with an evaluation of the analytical solution described in Section 4.

6. NUMERICAL EVALUATION

In all the numerical evaluations, we take $L = 6$, $m = 161$ and $n = 11$. Therefore, in the final computed oscillatory field there will be approximately six complete waves in the analysis

domain. Each complete wave will account for approximately 25 computational points. The hydrostatic zones at each end of the analysis domain are defined respectively by $1 \leq i \leq 14$ and $148 \leq i \leq 161$.

Throughout, 'standard' values for the non-dimensional parameters are taken in which $\lambda = 0.01$, $\mu = 100$ (implying $U = 10$) and $f = 20\pi$ (implying $t_p = 0.1$). The dimensionless time step is $\Delta t = 0.0025$ during the preliminary hydrostatic part of the integration. When the hydrodynamic pressure effects are included, $\Delta t = 0.00025$ in order to secure the convergence of the iterative parts of the calculation; there are then a total of 400 time steps per complete cycle of the oscillatory forcing prescribed in Equation (3.6).

The first part of the numerical experimentation is concerned with the case of a uniform equilibrium depth for which the analytical solution given in Section 4 is applicable. To obtain the solution, the governing equations, with a purely hydrostatic pressure balance, are first integrated ahead in time through 20 cycles. Subsequently, the hydrodynamic component of pressure is included and the equations are integrated for a further 13 cycles. The computed response is then oscillatory and the surface wave profile may be compared with an appropriate evaluation of Equation (4.1). In doing this, it is not possible to fix directly the values of ζ_a and ζ_b in terms of λ and μ. This is because the wave input into the numerical model involves propagation through a transitional hydrostatic zone. Accordingly, values of ζ_a and ζ_b have been adjusted so as to yield a fit with the numerically determined surface wave profile within the non-hydrostatic region. Figure 1 shows the computed wave profile over a horizontal segment of the analysis domain having an approximate length of 2 units (corresponding to

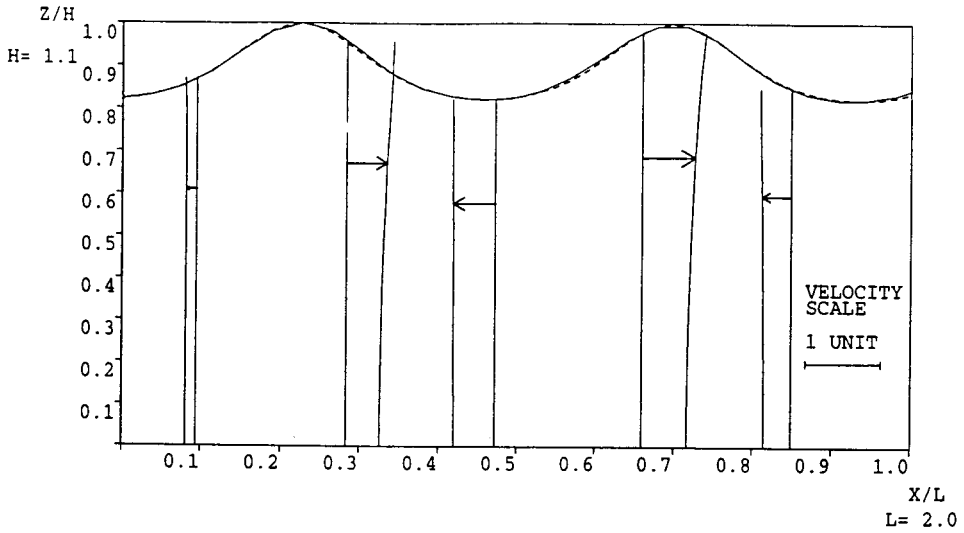

Figure 1. Free surface profile and velocity profiles for constant depth. The continuous lines refer to numerically determined profiles. The broken line refers to the analytically determined cnoidal wave profile.

$35 \leq i \leq 88$ and chosen to avoid possible contamination from the hydrostatic zones). This should be compared with the superimposed numerical evaluation of Equation (4.1) with $\zeta_a = 0.117$ and $\zeta_b = 0.0815$. This computation, in which the numerical solution of Equation (4.4) is obtained by the method of false position and the evaluation of Equations (4.5) and (4.6) by numerical integration, leads to $k = 0.878$, $\zeta_c = 0.141$ and $c = 0.946$. The overall comparison appears satisfactory and indicates that the selective smoothing procedures are not detrimental to the method of numerical solution.

Since the pressure is weakly non-hydrostatic, the wave-induced current will have an associated weak dependence on the depth co-ordinate. According to the cnoidal wave theory described in Reference [7], this dependence should be approximately quadratic in the depth co-ordinate. However, its precise determination from that theory involves a complicated evaluation of formulas connecting the Jacobian elliptic functions and is not pursued here. Nonetheless, the velocity profiles are a readily accessible part of the numerical solution and examples of these are also shown in Figure 1. Their approximate quadratic form is apparent and there is clear evidence that the bulk of the depth-variation is found immediately beneath the free surface.

It would clearly be desirable to be able to compare numerical results derived by the method described in this paper with an analytical solution describing wave propagation over a simple uneven topography. However, this would require an exact solution of a generalized KdV equation, which incorporates the effect of variable bottom topography. To the best of the authors' knowledge, such an analytical development and solution that complements the quoted case of a constant undisturbed depth is not available even for the most simple of topographies. Neither, for example, would it be appropriate to compare our results with a numerical integration of the generalized Green–Naghdi equations [15], since these were derived by making an assumption about the form of the fluid velocity beneath the waves. A feature of our method is that the velocity is determined and that the results are independent of the assumptions invoked in the development of reduced-dimension models. This will be of crucial importance in a subsequent generalization of the method to wave propagation in the presence of turbulent friction. It is in this case that a comparison with a relevant observational data set would be appropriate.

In Figure 2, we show profiles of the total hydrodynamic kinematic pressure Π calculated by

$$\Pi = \frac{\partial}{\partial t} \int_{\sigma}^{1} Hw \, \mathrm{d}\sigma + w\sigma \frac{\partial H}{\partial t} + P \tag{6.1}$$

From this, it is clear that Π is negative beneath the wave crests and positive beneath the troughs. In the analysis segment considered, the extremum values are -262 and 114 respectively. These values may be compared with the maximum hydrostatic pressure perturbation equal to $\mu\zeta_a/\lambda$, the computed value of which is 1170. Accordingly, the maximum hydrodynamic pressure amounts to about 22 per cent of the maximum hydrostatic pressure perturbation.

In the second experiment, we consider a non-uniform equilibrium depth which decreases from 1.0 to 0.25. The decrease is linear, and takes place between $i = 60$ and $i = 102$ (equivalent to about 1.5 wavelengths in water of unit equilibrium depth). In this case, we find that an

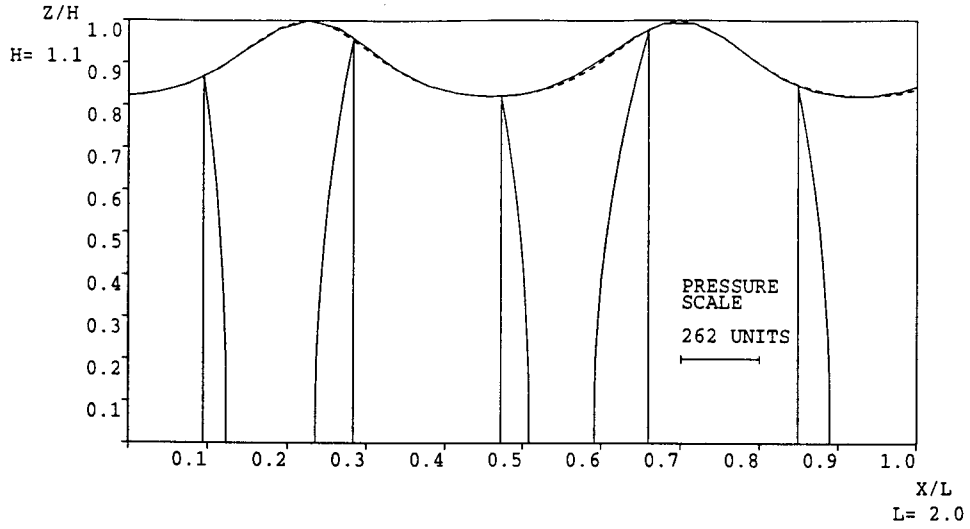

Figure 2. Profiles of the total hydrodynamic kinematic pressure for constant depth. The continuous lines refer to numerically determined profiles. The broken line refers to the analytically determined cnoidal wave profile.

effectively oscillatory wave response is obtained after 20 cycles of hydrostatic integration followed by three cycles of non-hydrostatic integration. Compared with the previous case, the short period of non-hydrostatic integration required now to achieve an oscillatory solution appears to be related to the presence of shallower water for $i > 102$. We present results in two sections of the analysis domain, which correspond to zones upstream and downstream of the region of depth reduction respectively.

Wave and velocity profiles in the two zones are shown in Figure 3. In Figure 3(a), we note that the upstream free surface profile appears to have a form characteristic of cnoidal waves propagating in water of constant equilibrium depth but with the expectation of a modulation caused by the upstream influence of the non-uniform topography. Radical changes in the wave profile are seen to occur only in the immediate neighbourhood of the region of reducing depth. In Figure 3(b), downstream of the depth reduction, the free surface profile again has the form of cnoidal waves in water of uniform equilibrium depth. Compared with the upstream zone, however, the height of the waves is reduced by about 26 per cent and their length by approximately 40 per cent. In such an inherently non-linear problem, it is not possible to express the wave solution as a superposition of an incident and reflected component as in References [1,2]. Nonetheless, the reduced wave height does suggest a substantial reflection of wave energy associated with the non-uniform bottom. This cannot, however, be interpreted in terms of a topographically induced perturbation to the near-bottom flow as in References [1,2].

In connection with the possible occurrence of the reflection of wave energy, it is pertinent to enquire whether a return of the equilibrium depth to its upstream value would result in a

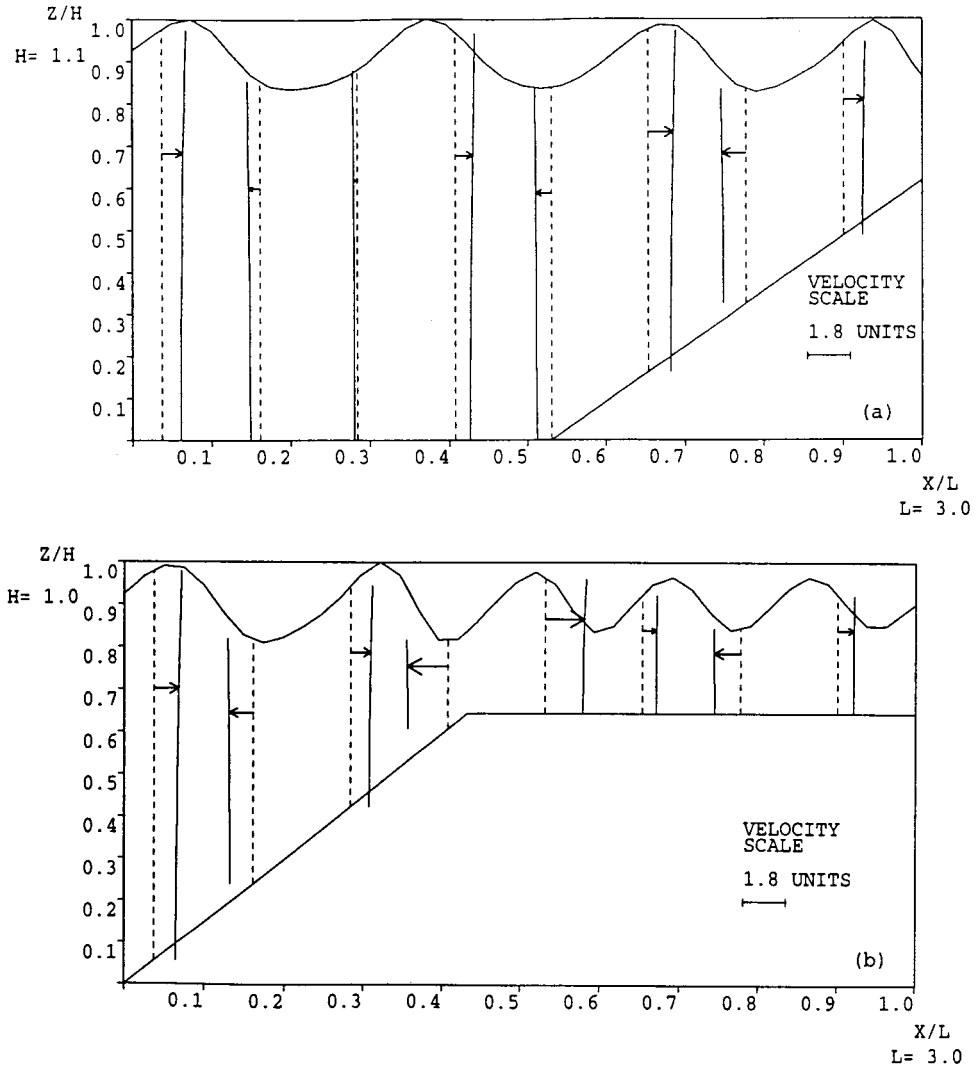

Figure 3. Free surface profile and velocity profiles for propagation over a linear decrease in depth. (a) Upstream of the depth change; (b) downstream of the depth change.

corresponding recovery of the wave height and wavelength. If this were in fact the case, the deforming effect of the topography would be purely local and would imply an absence of reflected wave energy. This question is addressed in a final experiment relating to propagation over an isolated bottom feature. Here, the equilibrium depth is defined by

$$h = 1 - 0.75 \sin\left\{\frac{\pi(i-60)}{42}\right\} \tag{6.2}$$

and it therefore represents a reduction in depth from 1 at $i = 60$ to 0.25 at $i = 81$, with a subsequent increase to 1 at $i = 102$. An effectively oscillatory wave response is obtained after 20 cycles of hydrostatic integration followed by 11 cycles of non-hydrostatic integration.

Wave and velocity profiles both upstream and downstream of bottom feature are shown in Figure 4. In Figure 4(a), we again note the classic cnoidal form of the wave profile upstream of the topographic feature. Above the region of depth reduction, the profile is radically deformed. Over the crest of the topography, there is a reduction in both the wave height and wavelength. The current velocities are fairly uniform with depth except above the topography where there is a noticeable increase in their magnitude just below the free surface.

In Figure 4(b), it is noteworthy that the free surface profile downstream of the topography does not fully recover its upstream form. Certainly, the wavelength returns to its approximate upstream value but the wave height is reduced by about 40 per cent. With this permanent change in height, the waves then propagate with an apparently classic cnoidal form towards the end of the analysis domain.

A reflection of wave energy by the bottom topography is, therefore, present and the effect of this on the overall free surface profile is shown for $15 \leq i \leq 148$ in Figure 5. In this, we delineate the profile for a non-uniform depth and superimpose on this the corresponding profile for a constant unit equilibrium depth. In general, there will be a phase difference between the waves in the two solutions. However, in this delineation, the relative position of the profiles has been adjusted so that the waves have an identical upstream phase. We note that the upstream influence of the topography is equivalent to a reduction in the height of the incoming waves by more than 10 per cent. This is consistent with a reflection from the topography reducing the net input of wave energy into the analysis domain. Downstream of the topography, the reduction in the wave height is accompanied by a marked phase shift in the waves relative to the far upstream value. Relative to the case of constant depth, the wave height is reduced by about 50 per cent.

7. CONCLUSIONS

A numerical method has been described which may be applied to compute the form of weakly non-hydrostatic free surface waves propagating over a general bottom topography. The efficacy of the method has been demonstrated by comparing the numerical solution for a constant equilibrium depth with the classic analytical solution for cnoidal waves. The comparison is deemed highly satisfactory. Two experiments are described relating to the propagation of a train of cnoidal waves over bottom topographical features. The deduction here is that cnoidal waves are deformed only in the immediate neighbourhood (approximately within one wavelength) of a change in equilibrium depth. In both experiments, an upstream reflection of wave energy takes place. The downstream transmitted waves consist of a train of classic cnoidal waves that propagate without change of form but with a reduced height and associated wavelength appropriate to the local equilibrium depth of the water.

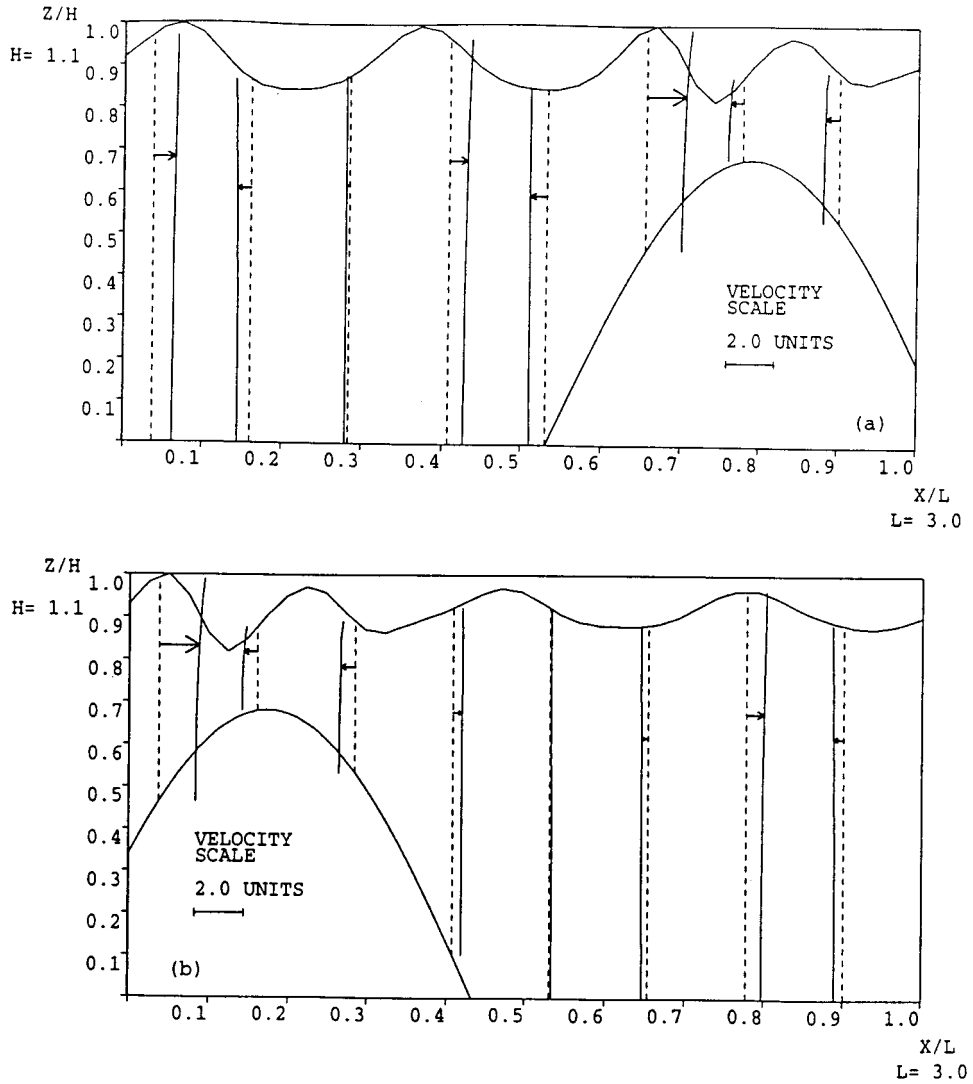

Figure 4. Free surface profile and velocity profiles for propagation over an isolated bottom feature. (a) Upstream of the depth change; (b) downstream of the depth change.

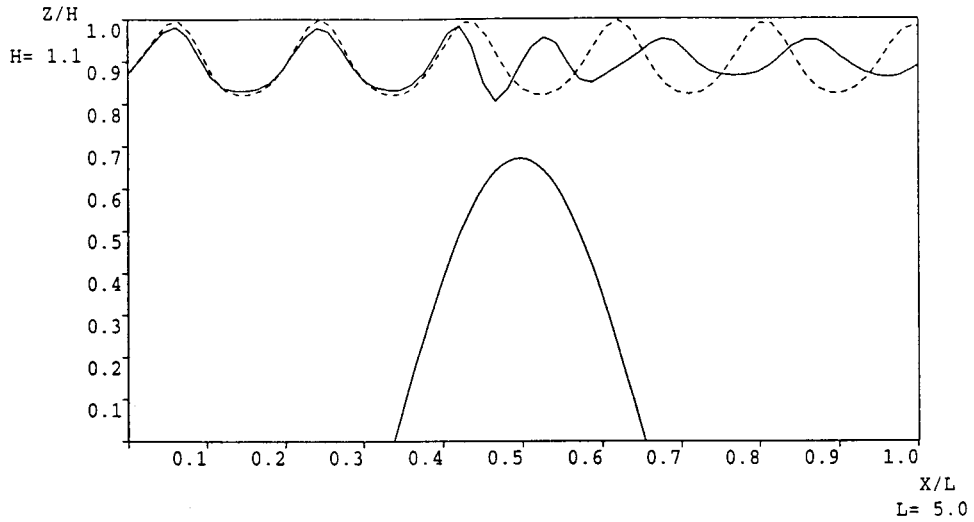

Figure 5. Free surface profile for propagation over an isolated bottom feature. The continuous line refers to numerically determined profile. The broken line refers to the profile determined in the case of a constant unit equilibrium depth.

APPENDIX A

The two smoothing procedures applied in the numerical method described in this paper are designed to eliminate any part of the developing response that appears in the shortest resolvable part of the solution spectrum. The procedures are selective and have a minimal influence on the response in the longer wavelength parts of the solution spectrum. The first of these, which is applied to both the ζ and $\tilde{\chi}$ fields every five time steps, eliminates identically that part of the response appearing as a two-grid increment wave. It has the form

$$\bar{X}_i = 0.0625\{-(X_{i-4} + X_{i+4}) + 4(X_{i-2} + X_{i+2}) + 10X_i\} \tag{A.1}$$

Here X denotes either of the field variables to be smoothed and $\bar{X}$ the smoothed resultant. The smoothing is applied only for those values of i consistent with $5 \leq i \leq 157$. Outside of this range, but with $i \geq 3$ and $i \leq 159$, a less selective smoother is applied in which

$$\bar{X}_i = 0.25(X_{i-2} + 2X_i + X_{i+2}) \tag{A.2}$$

The second of the smoothing operators is applied to the field of w after each iteration in the determination of the vertical velocity from Equations (5.12) and (5.13). The operator is designed to eliminate identically both the two- and three-grid increment waves that appear because of the generation of numerical noise in the iteration procedure. The smoothing operator is again selective and has a minimal effect on the longer wavelength components of

the spectrum, which contribute predominately to the physically relevant part of the solution. For each value of j, it is defined by

$$\bar{X}_i = 0.006944\{X_{i-8} + X_{i+8} - 8(X_{i-6} + X_{i+6}) + 3(X_{i-4} + X_{i+4}) + 44(X_{i-2} + X_{i+2}) + 64X_i\} \tag{A.3}$$

Here, the smoothing is applied only in the non-hydrostatic zone. Outside of this, $w \equiv 0$, the implication being that such values will be referenced when Equation (A.3) is applied immediately adjacent to the boundaries of the non-hydrostatic zone.

REFERENCES

1. Davies AG. The potential flow over ripples on the seabed. *Journal of Marine Research* 1979; **37**: 743–759.
2. Davies AG. On the interaction between surface waves and undulations on the seabed. *Journal of Marine Research* 1982; **40**: 331–368.
3. Newman JN. Propagation of water waves over an infinite step. *Journal of Fluid Mechanics* 1965; **23**: 399–415.
4. Miles JW. Surface-wave scattering matrix for a shelf. *Journal of Fluid Mechanics* 1967; **28**: 755–767.
5. Lighthill J. *Waves in Fluids*. Cambridge University Press: Cambridge, 1978.
6. Korteweg DJ, de Vries G. On the change of form of long waves advancing in a rectangular canal and on a new type of long stationary waves. *London*, *Dublin and Edinburgh Philosophical Magazine* 1895; **39**: 422–443.
7. Lamb H. *Hydrodynamics*. Cambridge University Press: Cambridge, 1932.
8. Johns B. The modelling of the free surface flow of water over topography. *Coastal Engineering* 1991; **15**: 257–278.
9. Nadiga BT, Margolin LG, Smolarkiewicz PK. Different approximations of shallow fluid flow over an obstacle. *Physics and Fluids* 1996; **8**: 2066–2077.
10. Li Z, Johns B. A three-dimensional numerical model of surface waves in the surf zone and longshore current generation over a plane beach. *Estuarine*, *Coastal and Shelf Science* 1998; **47**: 395–413.
11. Stansby PK, Zhou JG. Shallow-water solver with non-hydrostatic pressure: 2D vertical plane problems. *International Journal for Numerical Methods in Fluids* 1998; **28**: 541–563.
12. Stelling G, van Kester JATM. On the approximation of horizontal gradients in sigma co-ordinates for bathymetry with steep bottom slopes. *International Journal for Numerical Methods in Fluids* 1994; **18**: 915–935.
13. Whittaker ET, Watson GN. *A Course of Modern Analysis*. Cambridge University Press: Cambridge, 1958.
14. Sielecki A. An energy conserving scheme for the storm surge equations. *Monthly Weather Review* 1968; **96**: 150–156.
15. Green AE, Naghdi PM. A derivation of equations for wave propagation in water of variable depth. *Journal of Fluid Mechanics* 1976; **78**: 237–246.

